Applied Catalysis B: Environmental 165 (2015) 555–565

Contents lists available at ScienceDirect

Applied Catalysis B: Environmental

journal homepage: www.elsevier.com/locate/apcatb

Hydrogen-reduced Cu/ZnO composite as efficient reusable catalyst for diesel particulate matter oxidation

Grisel Corro[a,*], Surinam Cebada[a,1], Umapada Pal[b,2], Jose Luis García Fierro[c], Josefina Alvarado[d,3]

[a] Instituto de Ciencias, Benemérita Universidad Autónoma de Puebla, 4 sur 104, 72000 Puebla, Mexico
[b] Instituto de Física, Benemérita Universidad Autónoma de Puebla, Apdo. Postal J-48, 72570 Puebla, Mexico
[c] Instituto de Catálisis y Petroleoquímica, Cantoblanco, 28049 Madrid, Spain
[d] Departamento de Física, Universidad de Sonora, Hermosillo, Sonora, Mexico

ARTICLE INFO

Article history:
Received 14 May 2014
Received in revised form 15 October 2014
Accepted 19 October 2014
Available online 28 October 2014

Keywords:
Cu/ZnO composite catalyst
Diesel particulate matter oxidation
Cu^{1+}
Cold engine diesel emissions

ABSTRACT

Hydrogen-reduced copper-loaded ZnO (Cu/ZnO) showed a strong diesel particulate matter oxidation activity at temperature as low as 150 °C. Cu/ZnO catalyst with 5% nominal Cu content was tested for the oxidation of diesel particulate matter under air flow between 25 and 800 °C. The high catalytic performance of reduced 5%Cu/ZnO even after its use in diesel particulate matter oxidation has been assigned to the presence of Cu^{1+} ions at its surface, determined by Auger electronic spectroscopy. The high stability of Cu^{1+} could be assigned to the isoelectronic interaction of Cu^{1+} ($3d^{10}$) with Zn^{2+} ($3d^{10}$) at the Cu_2O–ZnO interface. Results presented in this work indicate that the composite catalyst can be considered as part of an exhaust catalytic system, for abating diesel particulate matter emission at low temperature.

1. Introduction

Finding efficient catalysts for the combustion of particulate matter emitted by diesel engines is one of the main tasks for protecting environment from toxic car-transport surges. The interest in diesel-engine exhaust after-treatment systems is ever-growing due to the increasingly stringent US and European emission standards. The main pollutants emitted from these engines are particulate matter and nitrogen oxides. Diesel particulates are hazardous environmental pollutants that account for a major fraction of fine air particulate matter in urban areas.

Diesel exhaust particles consist mainly of highly agglomerated solid carbonaceous material, volatile organic and sulfur compounds. Removal of the particulate matter containing polycyclic aromatic hydrocarbons from diesel-engine exhaust is a problem of great concern due to the well-known carcinogenic and mutagenic effects of these hydrocarbons [1–5]. Typically, the temperature of diesel exhaust remains between 120 and 360 °C at the start of cold engines, seldom exceeding this temperature in the positioned normal regime [6,7].

The diesel particulate filter (DPF) has so far been the most potential technological option for the effective control of diesel particulate matter emissions, where the particulate matter is trapped and periodically removed by combustion. However, the regeneration of DPF is a tedious process. The direct oxidation of particulate matter over the DPF requires high temperatures (~600 °C) and is generally carried out by injecting diesel into the exhaust, which results in an additional fuel consumption and thermal stress to the DPF. A catalytic diesel particulate filter is the best solution at present to reduce particulate matter emissions from diesel engines, where the particulate matter is trapped and oxidized with the help of a catalyst at temperatures below 600 °C. The only problem associated with this filter is the poor contact between the catalyst surface and the particulate matter [8,9]. Though several catalysts and technologies have been proposed to control this problem, the so-called fuel-borne catalysts (FBC), consisting in organometallic fuel additives, has seen to perform effectively in DPF, for the oxidation of particulate matter at lower temperatures [10,11]. However, the application of FBC is strongly restricted due to its continuous consumption and the accumulation of metal oxide as ash inside DPF. On the other hand, molten salt catalysts, which are generally considered as mobile catalysts, can wet the particulate matter surface,

* Corresponding author. Tel.: +52 22 2295500x7294.
E-mail addresses: griselda.corro@correo.buap.mx (G. Corro), upal@sirio.ifuap.buap.mx (U. Pal), jlgfierro@icp.csis.es (J.L.G. Fierro), josefina.alrive@gmail.com (J. Alvarado).
[1] Tel.: +52 22 2295500x7294.
[2] Tel.: +52 222 2295610.
[3] Tel.: +52 662 2684265.

http://dx.doi.org/10.1016/j.apcatb.2014.10.048
0926-3373/

causing a decrease of its oxidation temperature [12–17]. However, these catalysts have several drawbacks for practical applications due to their thermal degradation or selective leaching during particulate matter oxidation process.

Use of gaseous NO_2 in continuously regeneration trap technology, also results in a decrease in particulate matter oxidation temperature [18]. However, the present trend of reducing NO_x emission from diesel engines is the principal restriction for applying this technology. Therefore, diesel particulate matter oxidation by oxygen/air remains the focus of intense research to avoid the problems generated by all the above mentioned technologies.

Considerable success has been achieved on the development of new catalytic materials, and on understanding the possible mechanisms of direct oxidation of particulate matter by oxygen [19,20]. As the diesel-engine exhaust temperature is substantially lower than the particulate matter oxidation light-off temperature (between 550 and 650 °C), development of active catalytic materials is still a challenging issue, and demands further investigation on new catalytic materials. One of the common methods proposed for diesel particulate matter oxidation at lower temperature is the use of oxidation catalysts that reduce the combustion temperature of particulate matter down to the diesel exhaust temperature. During the last few years, several catalytic systems have been investigated for this purpose, and the diesel particulate matter oxidation temperature could be reduced to 200–400 °C [19–23] using these new catalysts. As far as our knowledge goes, particulate matter oxidation temperatures lower that 200 °C has not been achieved.

Most of the oxidation catalysts available in market are based on noble metals like Pt, Pd, and Rh, which are highly expensive and vulnerable to further price increase with their increasing demands. Therefore, research on noble-metal free catalysts or catalysts containing low amounts of noble metals are increasing worldwide. Copper-based catalysts have attracted much attention recently for heterogeneous catalysis not only for their economic advantage, but also for their high catalytic activity for NO reduction, CO and hydrocarbon oxidation, water-gas shift reaction, methanol synthesis and wet-oxidation of phenol [24–33]. Copper oxide (CuO) has been supported on different matrices for applications in many areas involving environmental catalysis [34,35], particularly for abatement of nitrogen oxide species or production of hydrogen from alcohols. On the other hand, Cu/ZnO catalysts have been widely used in many traditional applications such as in water-gas shift reaction [36,37], methanol synthesis [38–42], higher alcohol synthesis [43–45], methanol decomposition [46–50], partial oxidation of methanol [51–53], steam reforming of methanol [54–56], and photo-reduction of carbon dioxide with water [57].

Several research groups have studied the reduction kinetics of CuO/ZnO using conventional temperature-programmed reduction (TPR) methods [58,59,54,60]. Fierro et al. [60] have studied the reduction of CuO/ZnO with different Cu/Zn ratios, finding a promoting effect of ZnO on the reducibility of CuO. Time resolved XANES analysis of CuO/ZnO composite catalyst during oxidative reforming of methanol [61] could detect the formation of Cu^{1+} species as transient intermediate product during the reduction of Cu^{2+} to Cu^0. Oguchi et al. [62] have also detected Cu_2O as active species in steam reforming of methanol over CuO/ZnO catalysts. Formation of Cu^{1+} species has also been reported in Cu/ZnO catalysts utilized for methanol synthesis [63] and water-gas shift reaction [64,65].

In the present work, we have utilized hydrogen reduced Cu/ZnO composite as efficient catalyst for diesel particulate matter oxidation at low temperature, exploiting the interactions of transient and non-transient active copper species generated during its processing steps. The structural and electronic properties of the Cu/ZnO catalyst were studied utilizing X-ray diffraction (XRD), X-ray photoelectron spectroscopy (XPS), Auger electron spectroscopy ($Cu2p_{3/2}$, CuL_3MM) and UV–vis diffuse reflectance spectroscopy (DRS) techniques. The catalytic behavior of the Cu/ZnO composite in diesel particulate matter oxidation performed between 25 and 800 °C was correlated with its physicochemical properties, considering the contributions of active and non-active species like Cu^0, Cu^{1+}, and Cu^{2+} present on its surface.

2. Experimental

2.1. Catalysts

2.1.1. Catalyst preparation

ZnO powders obtained from Merck, Germany (99.9%) were impregnated with an appropriate amount of aqueous $Cu(NO_3)_2$ solution to incorporate a nominal 5 wt% of Cu in them. The suspension was stirred at room temperature for 1 h and dried at 120 °C overnight. After drying, the sample was reduced under pure H_2 flow (80 ml min^{-1}) at 450 °C for 4 h. The temperature of the furnace was increased at the rate of 10 °C min^{-1}. After cooling down the sample to 25 °C under H_2 flow, it was purged with air for 30 min, and stored in dry condition for its characterization.

A reference ZnO sample without $Cu(NO_3)_2$ solution was prepared in the same way. CuO powders (Merck, 99.9%), metallic unsupported copper particles (Baker, 99.9%, 0.59–1.00 mm) and metallic unsupported zinc particles (Baker, 99.9%, 0.59–1.00 mm) were also used as reference catalysts.

2.1.2. Catalyst characterization

A Quantachrome Nova-1000 sorptometer was used to measure the N_2 adsorption–desorption isotherms of the catalysts. Specific surface area (S_g) of the samples was estimated from their N_2 physisorptions at 77 K, using BET analysis methods. The samples (1 g each) were degassed at 400 °C for 2 h before recording their adsorption-desorption isotherms. After cooling to room temperature (25 °C), the isotherms were recorded in the pressure range of 0–6.6 kPa. The technique of back extrapolation of the linear portion of the isotherms to zero equilibrium pressure was used to determine the saturation uptake.

The diffuse reflectance spectra (DRS) of the catalyst before and after its 1st and 6th particulate matter oxidation cycles were measured on dry-pressed disk (~15 mm diameter) samples using a Varian Cary 500 UV-Vis spectrophotometer with DRA-CA-30I diffuse reflectance accessory, using $BaSO_4$ as standard reflectance sample. The crystallinity and structural phase of the samples were verified through powder X-ray diffraction (XRD), using the Cu Kα radiation (λ = 1.5406 Å) of a Bruker D8 Discover diffractometer. X-ray photoelectron spectra (XPS) were recorded on the freshly prepared hydrogen reduced 5%Cu/ZnO catalyst, after its 1st and 6th particulate matter oxidation cycles, using an Escalab 200R electron spectrometer equipped with a hemispherical analyzer, operating in a constant pass energy mode. Monochromatic Mg Kα emission ($h\nu$ = 1253.6 eV) from the X-ray tube operated at 10 mA and 12 kV was utilized for recording XPS spectra of the samples. Different energy regions of interest of the photoelectrons were scanned a number of times in order to get good signal-to-noise ratios. The intensities of the emission peaks were estimated by determining the integral of each peak after subtracting an S-shaped background and fitting the experimental peak to Lorenzian/Gaussian curves (80%L/20%G). The peak positions of the elements were corrected utilizing the position of C 1s peak coming from adventitious carbon appeared at 284.9 ± 0.2 eV.

2.2. Generation of diesel particulate matter

In this study, the term particulate matter has been used to refer both the soluble and insoluble (carbon) fractions of the diesel-emission. The particulate matter used in this study was generated

by burning pure Mexican diesel acquired from the market in a glass vessel, under controlled air flow as described in our previous work [66]. The emission from the exhaust of the vessel was directed to the catalyst sample (200 mg) placed inside a tubular quartz reactor (inner diameter 10 mm) in a programmable furnace. The process was performed using an air feed volume flow rate of 100 $cm^3\ min^{-1}$.

The particulate matter generated from the exhaust of the vessel was accumulated on the catalyst in the tubular reactor. The resulting contact between particulate matter and the catalyst in this case was considered similar to the contact between the particulate matter generated from a real diesel engine and the catalyst used in a particulate filter, and hence, the concept of tight mode or light mode contact between the particulate matter and the catalyst, used in several research studies, is of no significance.

After 1 h of diesel combustion, the total amount of particulate matter retained by the catalyst or by the quartz wool used for the blank experiment, was about 8.45 mg (measured using a Shimadzu AX200 balance), attaining a particulate-matter/catalyst-mass ratio of 0.042. Additional experiments were performed to determine the effect of higher particulate matter levels on the catalyst oxidation activity. The time of diesel combustion was increased to 2 h and 3 h, for attaining a particulate-matter/catalyst-mass ratio of 0.084 and 0.126, respectively.

To be sure that the combustion of diesel took place in lean conditions, oxygen feed volume flow in the vessel exhaust was monitored by gas chromatography. Oxygen flow remained higher than 10 $cm^3\ min^{-1}$ throughout the combustion process (oxygen in excess during diesel combustion). Organic functional groups present in the particulate matter were analyzed using a Bruker FT-IR spectrometer (Vertex 70) in the 800–4000 cm^{-1} spectral range. A thin, uniform KBr pellet prepared with 0.2 wt% of the particulate matter sample was used for recording the FT-IR spectra.

2.2.1. Oxidation of particulate matter through programmed temperature experiments

After 1 h of accumulation of diesel particulate matter over the catalyst surface, air was purged for 15 min to remove weakly attached combustion products. The air (20 vol.% of O_2 and 80 vol.% of N_2) flow rate was maintained at 100 $cm^3\ min^{-1}$. The mixture was then heated from room temperature (25 °C) to 800 °C at the rate of 10 °C min^{-1}. A thermocouple was inserted into the particulate matter–catalyst mixture to monitor its temperature along with the exothermic heat of the particulate matter oxidation. The emissions from the reactor were analyzed every 3 min through a computer-programmed Shimadzu gas chromatograph provided with a thermo-conductivity detector (TCD), to monitor the CO_2 evolution at different temperatures. The chromatograph used a Porapak column to analyze CO_2 evolutions as a function of the temperature of the particulate matter–catalyst mixture. The process comprising particulate matter accumulation on the catalyst at room temperature, its subsequent oxidation at high temperature, and then cooling down to 25 °C is named a cycle. The duration of each cycle was about 2.5 h (for 1 h of particulate matter accumulation). After the first cycle, five similar cycles were performed over the same catalyst sample. In order to determine the catalytic effect, an uncatalyzed particulate matter oxidation cycle was performed over only quartz wool at fixed temperatures between 25 and 800 °C.

3. Results and discussion

3.1. Characterization of diesel particulate matter

Fig. 1 shows the FT-IR spectra of the diesel particulate matter studied in this investigation. Principal characteristic peaks revealed in the spectrum correspond to the C—H asymmetric and symmetric stretching of aliphatic groups at 2953 cm^{-1}, 2923 cm^{-1} and 2853 cm^{-1}; C—O stretching of carbonyl groups at 1700 cm^{-1}; C=C stretching of aromatics and alkenes at 1560 cm^{-1}; and aliphatic C—H plane deformation of CH_2/CH_3 groups at 1450 cm^{-1} and 1380 cm^{-1} [67,68].

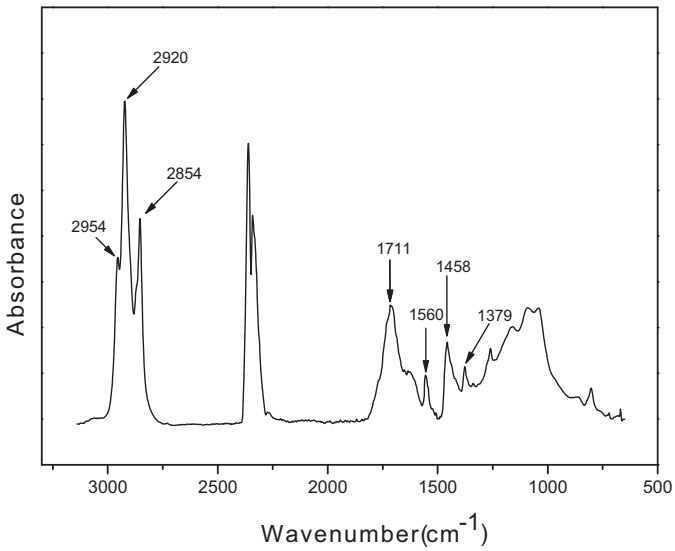

Fig. 1. FT-IR spectrum of diesel particulate matter sampled from the combustion vessel exhaust.

3.2. Characterization of the catalysts

The catalyst characterization data are summarized in Table 1. As can be seen, all the samples were of very low specific surface area, which do not change significantly after using them in particulate matter oxidation, even after several cycles.

3.2.1. X-ray diffraction of the catalysts

In Figs. 2 and 3, the powder XRD patterns of the hydrogen reduced Cu/ZnO catalyst before and after its use in particulate matter oxidation process (6 cycles) are presented, respectively. As can be seen, both samples revealed several well defined intense diffraction peaks corresponding to ZnO in hexagonal wurtzite phase (JCPDS#36-1451). There appeared two peaks of very low intensity at about 35.48° and 38.74° in the hydrogen reduced sample, which correspond to CuO in monoclinic (base-centered) phase (JCPDS#18-1916). While after using the catalyst for 6 cycles of particulate matter oxidation, the intensity of the XRD peaks associated to ZnO increased slightly, the intensity of the peaks associated to CuO increased substantially. There appeared no diffraction peak associated to metallic Cu in the hydrogen reduced catalyst before or after its use in particulate matter oxidation cycles. The XRD results presented above indicate that a major part of the incorporate copper remains in its divalent (Cu^{2+}) state.

Table 1
Catalyst characterization data.

Catalyst	Specific surface area ($m^2\ g^{-1}$)	
	Fresh sample	After 6 oxidation cycles
ZnO	4.52	4.51
CuO	5.22	5.14
5%Cu/ZnO	3.31	3.25

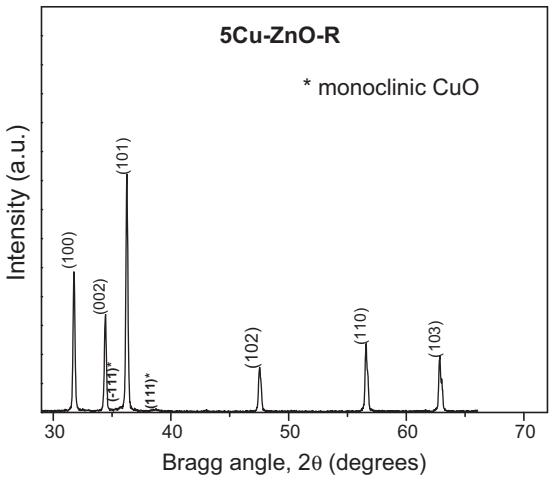

Fig. 2. XRD pattern of the Cu/ZnO catalyst with 5 wt% nominal Cu content after hydrogen reduction.

3.2.2. UV–vis characterization of the catalysts

3.2.2.1. Cu containing catalysts. The UV–vis absorption spectra of the metallic unsupported copper particles before and after their use in particulate matter oxidation process are presented in Fig. 4. The absorption spectrum of the fresh metallic unsupported copper particles (Fig. 4a) revealed several absorption bands. The band appeared in the 220–360 nm spectral range can be assigned to the charge transfer transition of the ligand O^{2-} to isolated metal center Cu^{2+} and the d–d transition in CuO particles [69–71]. The broad band spreading through 350–650 nm can be assigned to the overlapped absorption bands at around 400 and 510 nm, corresponding to the charge transfer transitions of O^{2-} and the hybridized 3d with 4s or 4p states of Cu^{1+} in Cu_2O [70,72,73], respectively. The band appeared between 530 and 650 nm is associated to the plasmonic absorption of metallic copper particles [74]. The weak signal appeared between 650 and 850 nm could be ascribed to the $^2E_g \rightarrow {}^2T_{2g}$ spin-allowed transitions of Cu^{2+} in the distorted octahedral symmetry [75]. The presence of CuO in the sample probably resulted from the reaction of atmospheric oxygen with the surface of the metallic unsupported copper particles.

The UV–vis absorption spectrum of the metallic unsupported copper particles after particulate matter oxidation cycles (Fig. 4b) shows a strong increase of absorption between 650 and 850 nm. Presence of this broad band associated to Cu^{2+} ions in distorted octahedral environment confirms the formation of CuO layer on metallic copper surface during particulate matter oxidation process [75]. Oxidation of metallic copper to form CuO during particulate matter oxidation process is clear when the absorption spectrum is compared with the absorption spectrum of a commercial CuO before (curve c of Fig. 4) and after its use in particulate matter oxidation cycles (curve d of Fig. 4). The position and intensity of the broad signal corresponding to CuO remained unchanged even after 6 oxidation cycles, suggesting a strong electronic stability of the Cu^{2+} species in CuO.

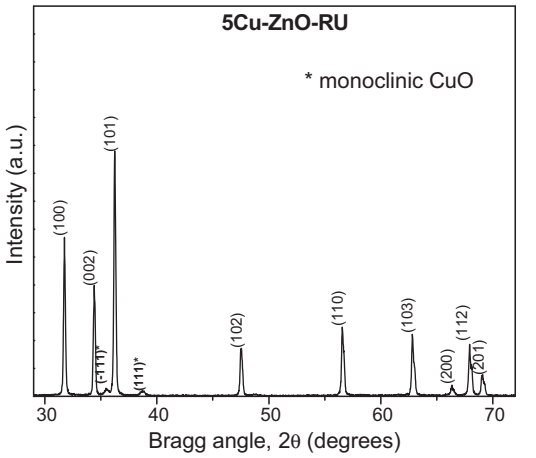

Fig. 3. XRD pattern of the hydrogen reduced Cu/ZnO catalyst containing 5 wt% nominal Cu, after 6 cycles of particulate matter oxidation.

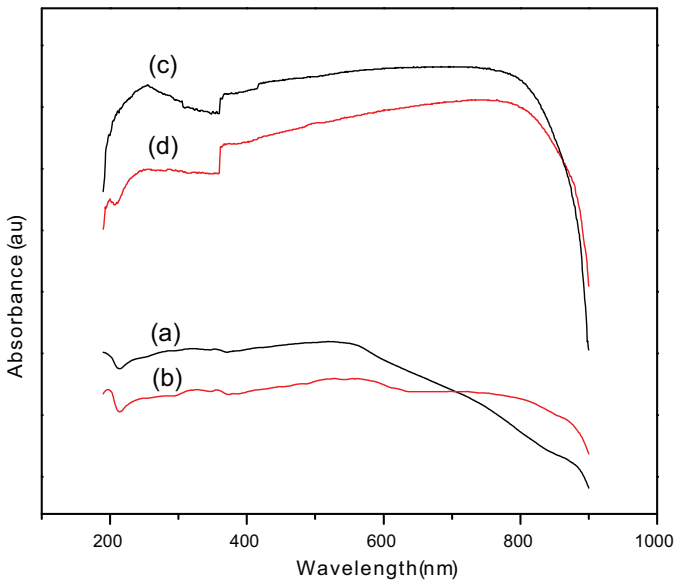

Fig. 4. Room temperature UV–vis absorption spectra of the (a) fresh metallic unsupported copper particles, (b) metallic unsupported copper particles after 6 oxidation cycles, (c) fresh commercial CuO, and (d) commercial CuO after 6 oxidation cycles. For clarity, the absorption spectra of the samples have been shifted vertically.

3.2.2.2. Zn containing catalysts. Fig. 5 shows the UV–vis absorption spectra of metallic unsupported zinc particles before and after its use in particulate matter oxidation cycles. As we can see (curve a of Fig. 5), the absorption spectrum of the fresh metallic unsupported zinc particles reveals a sharp peak centered around 232.4 nm with a tail toward longer wavelength side, which can be ascribed to the

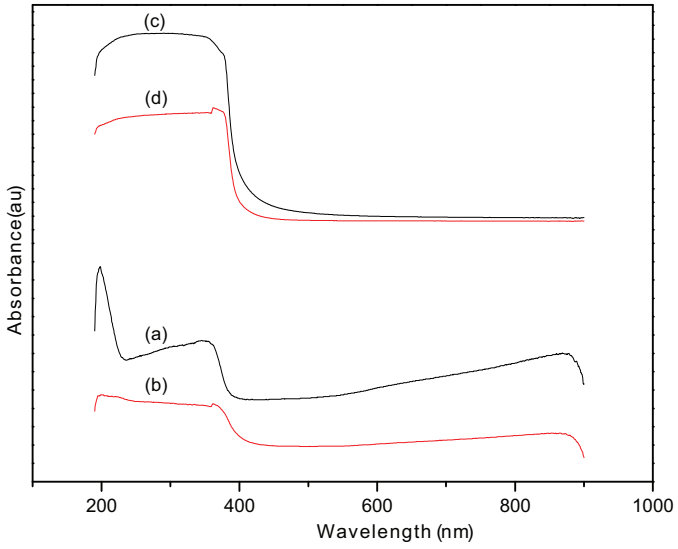

Fig. 5. UV–vis spectra of (a) fresh metallic unsupported zinc particles; (b) metallic unsupported zinc particles after 6 oxidation cycles; (c) fresh ZnO and (d) ZnO after 6 oxidation cycles.

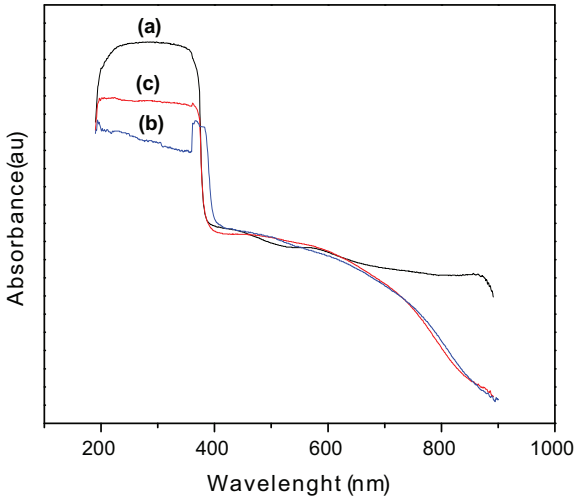

Fig. 6. UV–vis spectra of samples: (a) fresh 5%Cu/ZnO, (b) 5%Cu/ZnO after 1 oxidation cycle, and (c) 5%Cu/ZnO after 6 oxidation cycles.

surface plasmon absorption of metallic zinc [76]. The appearance of a broad absorption band in the 240–400 nm spectral region with a peak at around 350 nm might be due to the formation of a thin ZnO layer on metallic zinc surface. After 6 oxidation cycles (curve b of Fig. 5), the absorption band in 200–400 nm spectral region broadened and became more intense, indicating a growth of ZnO layers during diesel particulate matter oxidation.

The absorption spectra of pure ZnO sample before (curve c of Fig. 5) and after using it for 6 particulate matter oxidation cycles (curve d of Fig. 5) revealed similar absorption characteristics, with a strong absorption band between 200 nm and 400 nm, suggesting a good stability of the electronic properties of ZnO in high temperature.

3.2.2.3. 5%Cu/ZnO catalyst. Fig. 6 presents the UV–vis absorption spectra of the 5%Cu/ZnO catalyst before and after performing the 1st and 6th particulate matter oxidation cycles. The main features identified from the absorption spectrum of the hydrogen reduced 5%Cu/ZnO (curve a of Fig. 6) are: (i) a broad absorption signal between 200 nm and 400 nm with a sharp absorption edge at about 370 nm, corresponding to crystalline ZnO; (ii) a broad hump spreading through 400–510 nm associated to the absorption by Cu^{1+}; and (iii) a broad hump between 550 nm and 650 nm corresponding to the absorption due to metallic Cu [74].

The UV–vis absorption spectra of the 5%Cu/ZnO sample after performing the 1st and 6th oxidation cycles (curves b and c of Fig. 6) revealed apart from the absorption band edge of ZnO, a broad band spreading through 400–820 nm. This broad band appeared probably due to the overlapping of several low intensity bands like the absorption bands corresponding to Cu^{1+} ions (400 nm and 510 nm) [70], the plasmon absorption band of metallic copper between 350 and 650 nm [74], and the absorption band of Cu^{2+} ions in the higher wavelength side (650–850 nm) [69–71]. These results clearly indicate the oxidation of surface Cu atoms ($Cu \rightarrow Cu^{1+} \rightarrow Cu^{2+}$) during particulate matter oxidation process. The results obtained from optical characterization of the samples are in good agreement with the results obtained from their XPS analysis, presented in the following sub-section.

3.2.3. Characterization of the catalysts by XPS and Auger spectroscopy

3.2.3.1. $Cu2p_{3/2}$. As the binding energies of the $Cu2p_{3/2}$ core-level emissions from Cu^{1+} and Cu^0 are essentially the same, appearing at about 1.4 eV below that of Cu^{2+} ions, identification of both the

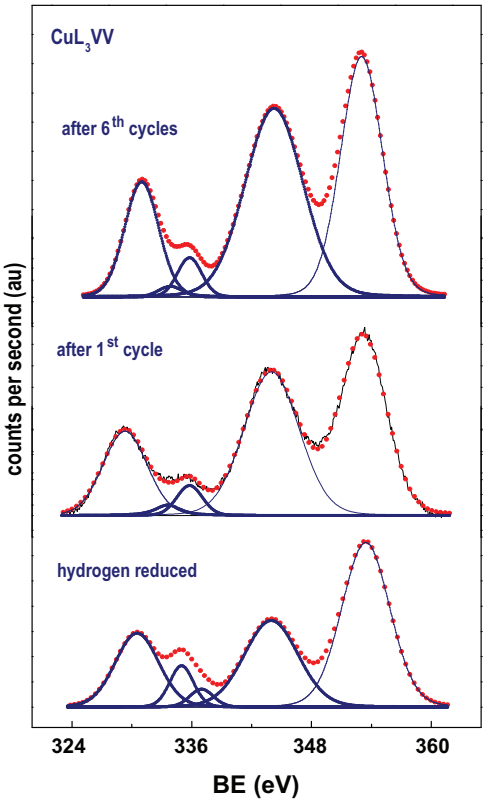

Fig. 7. CuL_3VV Auger transition of the catalysts.

reduced copper species (Cu^{1+} and/or Cu^0) in solid catalysts is very difficult by considering XPS data alone [77]. To identify these two copper species in our catalysts, we monitored their L_3VV X-ray induced Auger emissions (AES). For this purpose, the Auger parameter (α_A) was defined as:

$$\alpha_A = h\nu + (\text{BE Cu}2p_{3/2} - \text{BE Cu}_{\text{L3MM}})$$

where $h\nu$ is the energy of the incident photon (1253.6 eV) and BE $Cu2p_{3/2}$ and BE Cu_{L3MM} are the binding energies of the $Cu2p_{3/2}$ photoelectron and the L_3VV Auger emission, respectively.

The CuL_3VV Auger spectra of the freshly prepared hydrogen reduced catalyst, after its use in 1st oxidation cycle and 6th oxidation cycle are displayed in Fig. 7. It can be seen that the spectra are dominated by the ZnL_3VV Auger peaks that are located in the same energy region as of CuL_3VV. Notwithstanding, the peak fitting procedure allowed us to identify the CuL_3VV contribution. The values of α_A, the binding energies of $Zn2p_{3/2}$ and $Cu2p_{3/2}$ levels together and the Cu/Zn atomic ratios of the fresh reduced catalyst, and after its use in the 1st and 6th oxidation cycles of soot oxidation are compiled in Table 2.

The hydrogen reduced 5%Cu/ZnO catalyst, before using it in particulate matter oxidation, shows a binding energy (BE) of the $Cu2p_{3/2}$ emission of 932.7 eV (Fig. 8). This BE value and the absence of satellite line somewhere around 941 eV preclude the presence of Cu^{2+} ions. In other words, copper species must be either as Cu^0 and/or Cu^{1+}. The L_3VV Auger spectrum of the sample suggests that both Cu^0 and/or Cu^{1+} are present; although the metallic phase is dominant. On the other hand, the catalyst, after six particulate matter oxidation cycles, displays the BE of the $Cu2p_{3/2}$ level at 934.1 eV together with the intense satellite line. Both the facts indicate that copper remains essentially as CuO. This assignment is confirmed by the L_3VV Auger peak at 1851.1 eV with a minor contribution at 1849.1 eV, indicating that the major CuO species coexists with a minor proportion of Cu^{1+}. Finally, the BE of the sample 5%Cu/ZnO

Table 2
Binding energies (eV), Auger parameter (α_A) and Cu/Zn atomic ratios at the surface of the catalyst before and after using in diesel particulate matter oxidation.

Catalyst	$Zn2p_{3/2}$	$Cu2p_{3/2}$	α_A (eV)	Cu/Zn at
5%Cu/ZnO fresh	1020.82	932.7	1849.2 1851.0	0.461
5%Cu/ZnO after 1st cycle	1022.50	932.6 (85)[a] 934.1 (15)[a]	1849.5	0.318
5%Cu/ZnO after 6 cycles	1022.64	934.1	1849.1 1851.1	0.128

[a] Percentage peak area of each component presented in parenthesis.

after the 1st particulate matter oxidation cycle shows an intermediate behavior: a major contribution of reduced (Cu^{1+}/Cu^0) species and a minor contribution at CuO as confirmed by the small peak at a BE of 934.1 eV at its corresponding satellite structure. This tentative assignment is confirmed by a dominant L_3VV contribution whose Auger parameter fits with the expected value (1849.1 eV) for Cu_2O.

In addition, the Cu/Zn atomic ratio was calculated for the three samples and data are also collected in Table 2. It can be observed that the Cu/Zn atomic ratio at the catalyst surface reaches the maximum value (0.461) for the freshly prepared hydrogen reduced sample, whereas it drops substantially for the sample after the 1st particulate matter oxidation (0.318) and even more (0.128) after the 6th oxidation cycle. This observation indicates that sintering of Cu nanoparticles occurs during particulate matter oxidation.

3.2.3.2. $Zn2p_{3/2}$. The core level XPS spectra of the 5%Cu/ZnO catalyst in the $Zn2p_{3/2}$ emission region before and after its use in particulate matter oxidation cycles are shown in Fig. 9. The binding energies of the core electrons in the samples are presented in Table 2. The binding energy value of 1020.82 eV for the $Zn2p_{3/2}$ emission in the catalyst before its use in particulate matter oxidation process indicates the presence of reduced zinc (Zn^0) species on its surface [78]. On the other hand, the binding energy position of $Zn2p_{3/2}$ emission for the catalyst after using it in particulate matter oxidation, revealed a binding energy value of 1022.64 eV, indicating the presence of oxidized zinc at its surface, probably due to the formation of ZnO during oxidation cycles.

The presence of reduced zinc (Zn^0) species at the surface of the catalyst before using it in particulate matter oxidation cycles is expected as the catalyst was prepared by reducing it at high temperature in hydrogen atmosphere. It is well known that Zn^{2+} can be reduced in hydrogen atmosphere only at temperatures above 600 °C [79]. However, we reduced the catalyst (5%Cu/ZnO) at 450 °C in hydrogen before using it for particulate matter oxidation cycles. As the copper can be reduced between 150 and 300 °C in hydrogen [80,81], during our reduction process, a fraction of copper gets reduced to metallic copper (Cu^0) which might have catalyzed the reduction of ZnO to Zn^0 at least at the catalyst surface according to the reaction:

$$ZnO + H_2 \xrightarrow{Cu^0} Zn^0 + H_2O \quad (1)$$

as has been proposed by Okamoto et al. [82] for their reduced CuO–ZnO catalysts.

It is interesting to note (Table 2) that the Cu/Zn atomic ratio at the surface of the fresh hydrogen reduced catalyst is higher (0.461) than the value estimated (0.128) after its use in 6 oxidation cycles. The decrease of Cu/Zn ratio in the catalyst after its use in particulate matter oxidation cycles can be understood if we consider an increase in size of the Cu particles due to agglomeration during oxidation cycles performed at high temperature. The increase in the size of the Cu particles results in a decrease in net surface Cu atoms. Now, this decrease of surface Cu atoms should have reduced the catalytic activity of the composite catalyst for the particulate matter oxidation reaction. However, as can be seen from the catalytic performance of the catalyst discussed in the next sub-section, this is not the case. These results are not at all surprising as the particulate matter oxidation process generates Cu^{1+} sites, which are active

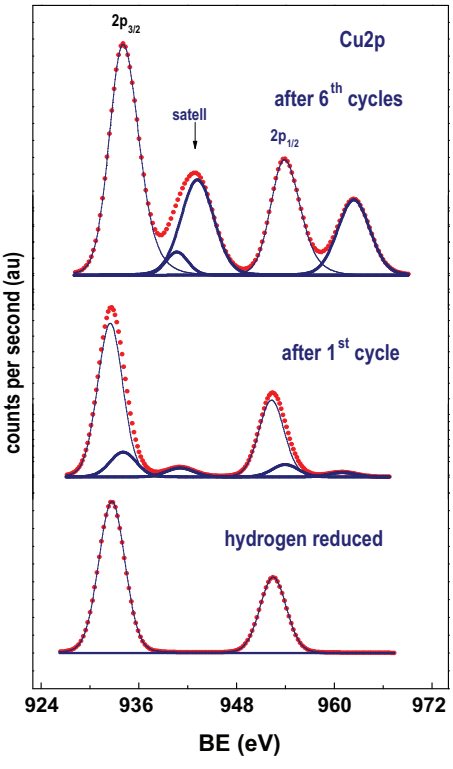

Fig. 8. $Cu2p_{3/2}$ core level XPS spectrum of 5%Cu/ZnO.

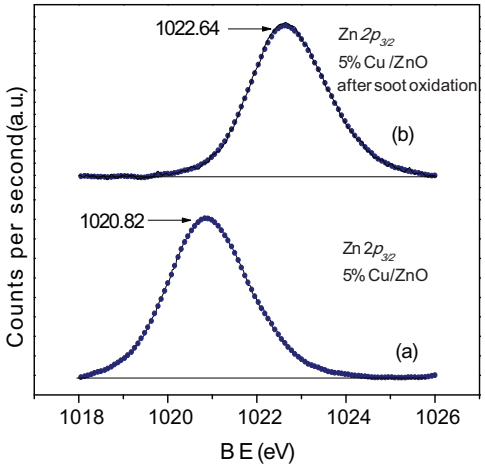

Fig. 9. $Zn2p_{3/2}$ core level XPS spectra of 5%Cu/ZnO: (a) before particulate matter oxidation cycles and (b) after particulate matter oxidation cycles.

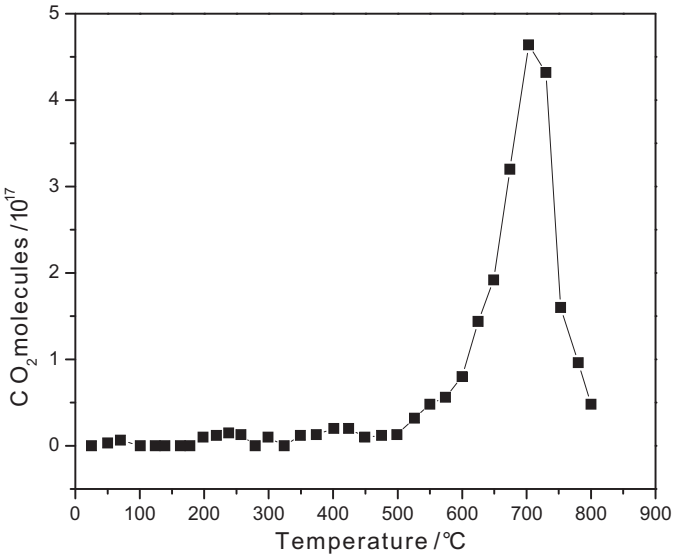

Fig. 10. Evolution of CO_2 molecules as a function of particulate matter oxidation temperature over quartz wool.

for particulate matter oxidation, compensating the loss of surface atoms of the Cu particles.

3.3. Particulate matter oxidation over the catalysts

3.3.1. Particulate matter oxidation over quartz wool

Fig. 10 shows the effect of temperature on particulate matter oxidation over quartz wool. As can be seen, only one signal of CO_2 evolution was revealed between 550 and 800 °C, peaked at about 700 °C. Only a very small amount of CO_2 could be detected during the particulate matter oxidation reaction at temperatures between 25 and 600 °C.

3.3.2. Particulate matter oxidation over metallic unsupported copper particles

The evolution of CO_2 during particulate matter oxidation over metallic unsupported copper particles during successive cycles is presented in Fig. 11. As can be seen, during the first cycle, there is a strong CO_2 signal at about 250 °C. However, this signal disappeared almost completely during the subsequent oxidation cycles, indicating a complete deactivation of the catalyst. The effect is expected as

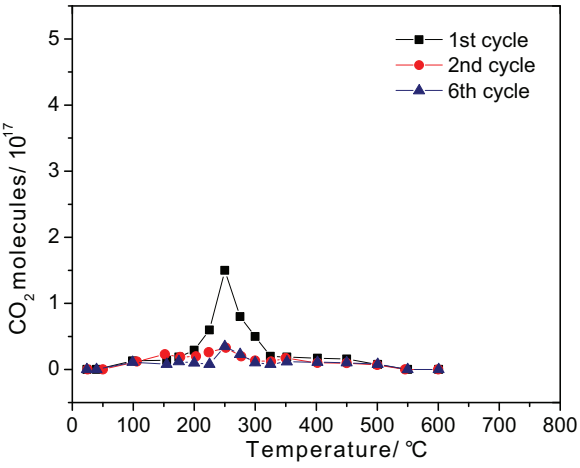

Fig. 11. Evolution of CO_2 molecules as a function of particulate matter oxidation temperature over metallic unsupported copper particles.

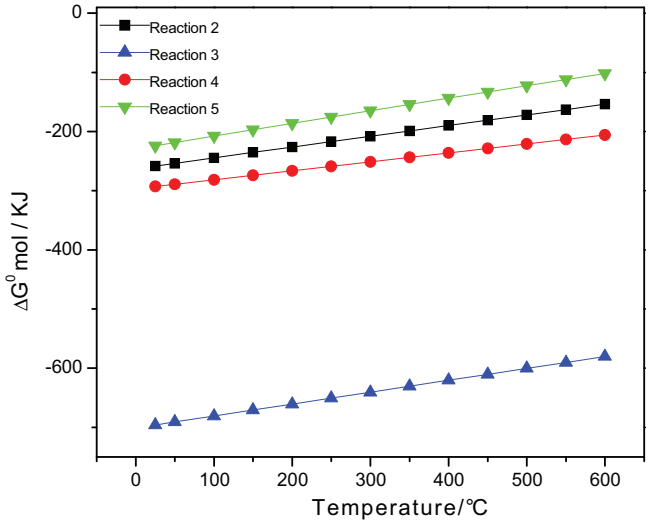

Fig. 12. ΔG^0 values calculated for the reactions: (2) $2Cu^0 + O_2 \rightarrow 2CuO$; (3) $2Zn^0 + O_2 \rightarrow 2ZnO$; (4) $4Cu^0 + O_2 \rightarrow 2Cu_2O$; (5) $2Cu_2O + O_2 \rightarrow 4CuO$.

the electronic state of metallic copper changes at high temperature under excess oxygen flow utilized for particulate matter oxidation, converting most of the active metallic catalytic sites to non-active sites for diesel particulate matter oxidation according to the reaction:

$$2Cu^0 + O_2 \rightarrow 2CuO \quad (2)$$

The ΔG^0 values calculated for the reaction (2) and all other possible oxidation reactions of copper and zinc are presented graphically in Fig. 12, for the whole temperature range used for particulate matter oxidation. The negative estimated values of ΔG^0 indicate all the reactions (reactions (2)–(5)) can take place spontaneously in the used temperature range.

The UV–vis absorption spectra of the metallic unsupported copper particles before and after their use in particulate matter oxidation cycles (Fig. 4) are in good agreement with the calculated ΔG^0 values of the possible oxidation reactions of copper. Absorption spectrum of the catalyst before particulate matter oxidation reaction revealed the presence of reduced copper (Cu^0), which can generate the superoxide O_2^- ions, the highly active species well known for improving the oxidation of diesel particulate matter [83,84]. The broad signal appeared in the 650–850 nm range for the catalyst after six oxidation cycles is associated to CuO [69–71]. As it is well known, CuO does not have the capacity of adsorbing oxygen, and presents very low activity for particulate matter oxidation, as has been shown by Lopez-Suarez et al. [85]. It is interesting to note that the absorption band appeared between 530 nm and 650 nm, corresponding to the Cu^0 plasmon absorption [74], remained unaffected by the particulate matter oxidation process, indicating the presence of metallic copper inside the metallic unsupported copper particles despite being in strong oxidation conditions. However, the surface CuO layer built-up over Cu^0 during the first oxidation cycle would have acted as a barrier for the interaction of diesel particulate matter and/or O_2 with the inner Cu^0 sites.

In a recent study [66], we demonstrated that 3%Ag/SiO_2 is a very active, highly stable catalyst for diesel particulate matter oxidation at temperatures around 250 °C. The high activity and stability of this catalyst have been associated to the presence of silver species at the surface of the catalyst, which remain in metallic state, despite the severe oxidation conditions of the reaction. Metallic silver (Ag^0) was considered to promote the formation of superoxide ions (O_2^-) resulting in an enhancement of diesel particulate matter oxidation rate, in a similar way as Cu^0 might have generated O_2^- at the

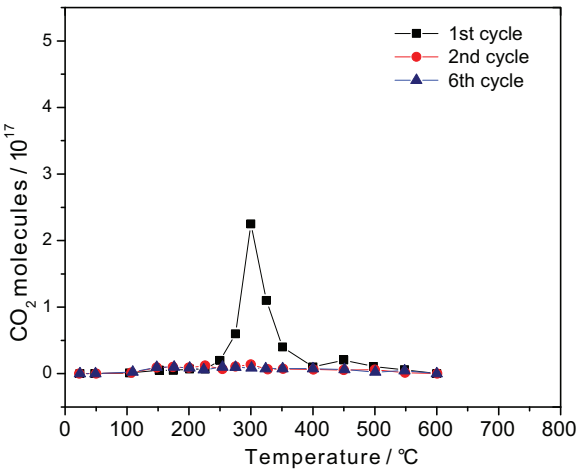

Fig. 13. Evolution of CO_2 molecules/g cat as a function of particulate matter oxidation temperature over metallic unsupported zinc particles.

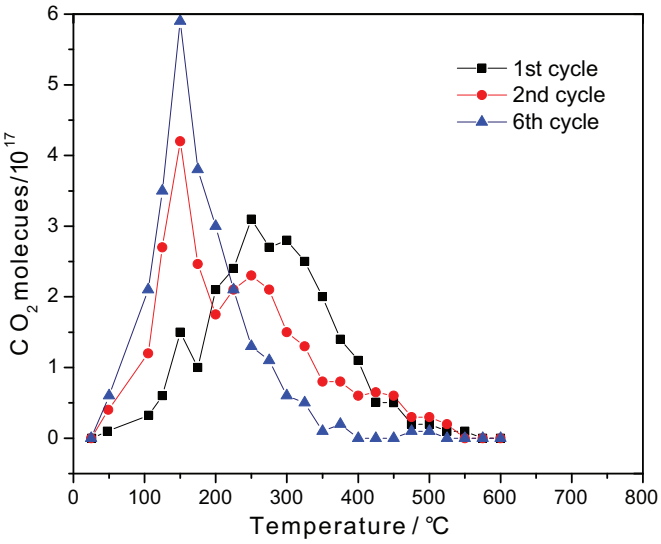

Fig. 14. Evolution of CO_2 molecules/g cat as a function of particulate matter oxidation temperature over 5%Cu/ZnO.

metallic unsupported copper particles surface in the present case. The evolution of CO_2 with temperature for the diesel particulate matter oxidation during 6 reaction cycles catalyzed by 3%Ag/SiO_2 showed a similar profile as the evolution of CO_2 measured during the first diesel particulate matter oxidation cycle catalyzed by the metallic unsupported copper particles. This similarity suggests a similar reaction path for diesel particulate matter oxidation by the superoxide ions promoted by Ag^0 or Cu^0 species in the two cases.

3.3.3. Particulate matter oxidation over commercial CuO

In order to confirm the assumption that CuO is not active for particulate matter oxidation process, we investigated the activity of a commercial CuO for diesel particulate matter oxidation. The evolutions of CO_2 with the increase of temperature during 6 oxidation cycles (results not shown) revealed only a very small amount of CO_2 evolution at about 500 °C. These results demonstrate that CuO is not active for oxidizing diesel particulate matter.

3.3.4. Particulate matter oxidation over the metallic unsupported zinc particles

The evolution of CO_2 during particulate matter oxidation over the metallic unsupported zinc particles is shown in Fig. 13. As we can see, there appeared an intense CO_2 evolution signal at about 300 °C during the first particulate matter oxidation cycle. However, this signal disappeared almost completely during the subsequent reaction cycles, indicating a complete deactivation of the catalyst during the first cycle of diesel particulate matter oxidation.

The result is not at all unexpected as metallic zinc gets oxidized to form ZnO at the high temperature used for particulate matter oxidation in presence of abundant oxygen. While the produced ZnO is not active for diesel particulate matter oxidation, formation of ZnO layer at the surface of the unsupported metallic zinc particles prevent them to participate in the oxidation process. Formation of ZnO during the particulate matter oxidation cycles over the metallic unsupported zinc particles has also been verified by their UV–vis absorption spectra before and after the particulate matter oxidation cycles (Fig. 5). In the absorption spectrum of the catalyst used for particulate matter oxidation cycles, the signal due to ZnO (between 200 and 400 nm) increased drastically, indicating a strong oxidation of metallic zinc particles. The possibility of this spontaneous reaction can be perceived from the ΔG^0 values (Fig. 12) estimated for reaction (3) in the whole temperature range used for particulate matter oxidation process:

$$2Zn^0 + O_2 \rightarrow 2ZnO \quad (3)$$

3.3.5. Particulate matter oxidation over ZnO

The results of diesel particulate matter oxidation over ZnO at different temperatures revealed (not shown) a very small amount of CO_2 evolution during all the six oxidation cycles. As the UV–vis absorption spectra of the catalyst (Fig. 5) before and after its use in particulate matter oxidation cycles remained almost unchanged, we can consider that the compositional stoichiometry or electronic structure of ZnO remained unaffected even after 6 particulate matter oxidation cycles.

3.3.6. Particulate matter oxidation over hydrogen reduced 5%Cu/ZnO catalyst

Fig. 14 shows the temperature evolution of CO_2 during particulate matter oxidation over the hydrogen reduced 5%Cu/ZnO catalyst. The CO_2 evolution characteristics during each cycle of particulate matter oxidation are discussed below:

During the 1st oxidation cycle:

The CO_2 evolution curve revealed a broad signal spreading through 200–550 °C, which can be assigned to the overlapping of two signals: a signal at about 250 °C arising from the particulate matter oxidation over metallic copper (as was demonstrated for the particulate matter oxidation over metallic unsupported copper particles in Fig. 11), and another signal at about 300 °C associated to the particulate matter oxidation over metallic zinc (as was demonstrated for the particulate matter oxidation over metallic unsupported zinc particles in Fig. 13). Further, the intensity of both signals (at 250 °C and 300 °C) are higher than the signals observed for Cu (Fig. 11) and for Zn (Fig. 13), indicating the presence of Cu^0 and Zn^0 particles in higher amounts at the surface of the composite catalyst which might have been formed during its preparation. It is interesting to note a small signal which appeared at about 150 °C. This signal was not detected during particulate matter oxidation over the other catalysts (metallic unsupported copper particles, CuO, metallic unsupported zinc particles, and ZnO). Now, the catalyst composition determined by the core level XPS spectra, and the values of the Auger parameter α_A revealed the presence of Cu^0, Zn^0, Cu^{2+}, Zn^{2+}, and Cu^{1+} species in the hydrogen reduced 5%Cu/ZnO catalyst before its use in particulate matter oxidation process, however, the observed CO_2 evolution signal at about 150 °C cannot be associated to the particulate matter oxidation over Cu^0, or Zn^0 sites,

as they present oxidation activities at higher temperatures (250 °C and 300 °C, respectively). This signal can neither be associated to the particulate matter oxidation over Cu^{2+} or Zn^{2+} species, since CuO and ZnO are inactive for the reaction. We assign CO_2 evolution signal detected at 150 °C to the particulate matter oxidation over Cu^{1+} ions present in the hydrogen reduced composite catalyst. As has been demonstrated earlier, the freshly prepared hydrogen reduced 5%Cu/ZnO sample contains Cu^{1+} ions, revealing corresponding absorption band between 400 nm and 510 nm (curve a, Fig. 6), and Auger parameter α_A of 1849.5 eV corresponding to Cu_2O (discussed in Section 3.2.3).

It is worth noting that the particulate matter used in this study contains both the insoluble (carbon) and soluble organic fraction (SOF) components. We associate the CO_2 evolution peak detected at 150 °C to the catalytic oxidation of both the SOF and insoluble carbonous components over the composite catalyst through Cu^{1+} active species. In fact there appeared no other peak of CO_2 evolution by extending the particulate matter oxidation temperature up to 800 °C while using our composite catalyst. We believe that the oxidation of the insoluble carbon of particulate matter in close contact with Cu^{1+} ions is promoted by the exothermic heat of SOF catalytic oxidation at the surface of the catalyst particles.

During the 2nd to 6th cycles:

The intensity of the CO_2 evolution signal attributed to particulate matter oxidation over Cu^{1+} increases strongly from cycle to cycle (Fig. 14), suggesting a gradual increase of Cu^{1+} concentration at the catalyst surface in each oxidation cycle. An enhanced oxidation of SOF at the Cu^{1+} sites of the catalyst along with the promoting effect of the exothermic heat of SOF oxidation might be the reasons for the higher CO_2 evolution signals observed in the successive oxidation cycles.

The CO_2 evolution signals detected at about 250 °C and 300 °C for the 1st cycle (due to particulate matter oxidation over Zn^0 and Cu^0, respectively) decrease gradually from cycle to cycle due to the oxidation of metallic zinc and metallic copper at the surface of the catalyst. While the Zn^0 present in freshly prepared hydrogen reduced catalyst gets oxidized to Zn^{2+} following Eq. (3), Cu^0 species present in the catalyst get oxidized to Cu^{1+} during the oxidation cycles following the reaction:

$$4Cu^0 + O_2 \rightarrow 2Cu_2O \quad (4)$$

Following Eq. (4), the concentration of Cu^{1+} species over the catalyst surface increases in expense of Cu^0 on repeating the oxidation cycles, increasing CO_2 evolution at 150 °C, and suppressing the signal at 250 °C. The conclusion is supported by the CuL_3VV Auger spectra displayed in Fig. 7 and the Auger parameter reported in Table 2, which show for the 5%Cu/ZnO catalyst after 6 particulate matter oxidation cycles a dominant L_3VV contribution, whose Auger parameter fits the expected value for Cu_2O (1849.5 eV).

We must take into consideration that both Cu^0 and Cu^{1+} could be oxidized to form Cu^{2+} in the used oxidation conditions according to the reactions:

$$2Cu^0 + O_2 \rightarrow 2CuO, \quad (2)$$

and

$$2Cu_2O + O_2 \rightarrow 4CuO \quad (5)$$

The ΔG^0 values for these reactions (Fig. 12) also suggest that both reactions can take place spontaneously in the temperature range used for particulate matter oxidation in this study. However, as the results presented above indicate, the fraction of Cu^{1+} oxidized to form Cu^{2+} (reaction (5)) in our hydrogen reduced 5%Cu/ZnO catalyst during particulate matter oxidation is very low, i.e. the Cu^{1+} ions are highly stable in the used oxidation conditions. The high stability of Cu^{1+} ions in the severe oxidation conditions of particulate matter oxidation cycles can be understood considering the isoelectronic interactions between Cu^{1+} ($3d^{10}$) with Zn^{2+} ($3d^{10}$) at the Cu_2O–ZnO interface as has been explained by Herman et al. [86].

As can be observed from Fig. 10, a very small amount of CO_2 can be generated through particulate matter oxidation between 25 and 600 °C in absence of an oxidation catalyst. To estimate the catalytic activity of our hydrogen reduced Cu/ZnO composite, CO_2 evolution during particulate matter oxidation in absence of the catalyst was monitored on particulate matter deposited on quartz wool between 25 and 800 °C. The total area under the CO_2 evolution curve between 25 and 800 °C $[CO_2]_{Ref}$ was considered as a measure of the total amount of carbon in the particulate matter, generated from the exhaust gas of the vessel and accumulated for 1 h. The catalytic efficiency of the catalyst was calculated from the ratio of $[CO_2]$ evolved during the catalytic process and the same in absence of the catalyst (using only quartz wool) as:

$$\text{Catalyst efficiency} = \frac{[CO_2]_{Cat}}{[CO_2]_{Ref}},$$

where $[CO_2]_{Cat}$ is the area under CO_2 evolution curve (between 25 °C and 800 °C) during particulate matter oxidation over the catalyst, and $[CO_2]_{Ref}$ is the area under CO_2 evolution curve during particulate matter oxidation over quartz wool. The $[CO_2]_{Cat}$ and calculated catalytic efficiency values for the 5%Cu/ZnO catalyst for different oxidation cycles have been presented in Table 3. The results obtained from the catalytic evaluation of our hydrogen reduced 5%Cu/ZnO composite indicate clearly that the catalyst remains active even after six cycles of particulate matter oxidation, and the oxidation temperature remains as low as 150 °C.

To verify the effect of soot loading on the oxidation performance of the catalyst, we deposited different amounts of soot on the surface of a fixed amount of catalyst to obtain particulate-matter/catalyst-mass ratios of 0.084 and 0.126. The CO_2 evolutions during particulate matter oxidation over 5%Cu/ZnO in its 6th cycle for the particulate-matter/catalyst-mass ratios of 0.042, 0.084, and 0.126 are shown in Fig. 15. As can be seen, though the intensity of CO_2 evolution attributed to particulate matter oxidation over Cu^{1+} (at about 150 °C) increases with the particulate-matter/catalyst-mass ratio, the peak position of CO_2 evolution shifts gradually toward higher temperature with higher soot loading. While the increase in CO_2 evolution intensity for higher soot loading can be associated to an increased amount of soot in contact with the catalyst, and the transfer of a huge exothermic heat generated

Table 3
CO_2 evolution, and estimated efficiency of the composite catalyst for the 1st, 2nd, and 6th oxidation cycles of PM oxidation.

Catalyst	Intensity of CO_2 evolution (10^{18} molecules)			Catalyst efficiency		
	1st	2nd	6th	1st	2nd	6th
Quartz wool	627					
5%Cu/ZnO	617	598	613	0.98	0.95	0.97

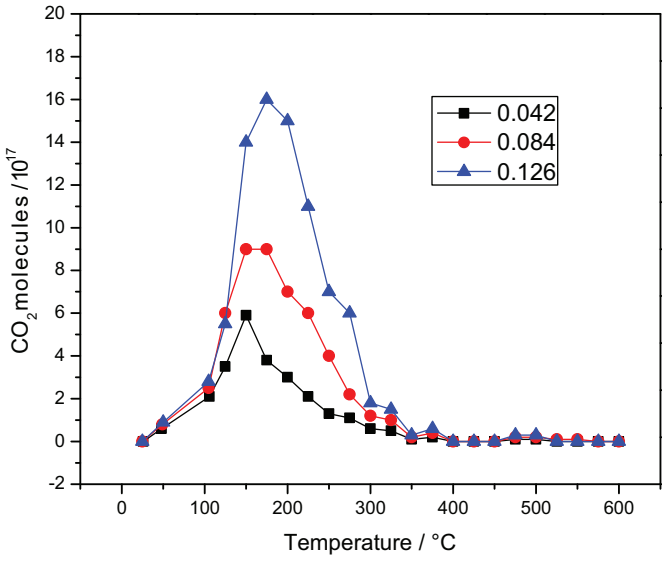

Fig. 15. Evolution of CO_2 molecules/g cat as a function of particulate matter oxidation temperature over 5%Cu/ZnO, its 6th cycle for different particulate-matter/catalyst-mass ratios.

during soot oxidation to the neighboring particulate matter molecules, the high temperature shift of the oxidation peak is probably due to the full coverage of catalyst surface for higher soot loading (not all the particulate matter molecules might be in contact with the catalyst). While a higher particulate matter loading on the catalyst generates higher amount of CO_2 due to the oxidation of higher number of particulate matter molecules, the oxidation activity of the composite catalyst remains unaffected. Such characteristics of the composite catalyst indicate that it can be considered as the part of an exhaust catalytic system, for abating diesel particulate matter emission at low temperature.

4. Conclusions

A low cost, high performance catalyst for diesel particulate matter oxidation could be synthetized by hydrogen reduction of Cu loaded ZnO powders. Using the catalyst, the oxidation temperature of diesel particulate matter in air could be lowered to 150 °C. The catalyst can be used for the abatement of diesel engine emissions even from the starting moment of a cold engine. The electronic properties of the composite catalyst evaluated through XPS and AES revealed that even after 6 oxidation cycles between 25 and 800 °C, the concentration of Cu^{1+} species at the catalyst surface does not decrease due to the isoelectronic interactions of Cu^{1+} ($3d^{10}$) with Zn^{2+} ($3d^{10}$) at the Cu_2O–ZnO interface. On the other hand, during the first few cycles of soot oxidation at high temperature, the concentration of surface Cu^{1+} species can increase, which in turn increases the efficiency of the catalyst over oxidation cycles.

The results obtained from diesel particulate matter oxidation activity and electronic state analysis of incorporated copper in the composite catalyst suggest that the Cu^{1+} ions at the catalyst surface act as active species for particulate matter oxidation due to their favorable electronic configuration.

Acknowledgements

The authors acknowledge VIEP & DITCo, BUAP (Grants # VIEP 45/NAT/2014, and INOVACION #3 and #19), and CONACyT, Mexico (Grant # CB-2010/151767) for their financial supports.

References

[1] J. Liu, Z. Zhao, J. Wang, C. Xu, A. Duan, G. Jiang, Q. Yang, Appl. Catal. B 84 (2008) 185–195.
[2] D. Gamarra, C. Belver, M. Fernandez-Garcia, A. Martinez-Arias, J. Am. Chem. Soc. 129 (2007) 12064–12065.
[3] M. Machida, Y. Murata, K. Kishikawa, D. Zhang, K. Ikeue, Chem. Mater. 20 (2008) 4489–4494.
[4] L. Zhu, J. Yu, X. Wang, J. Hazard. Mater. 140 (2007) 205–210.
[5] B.M. Reddy, K.N. Rao, Catal. Commun. 10 (2009) 2247–2268.
[6] B.R. Stanmore, J.F. Brilhas, P. Gilot, Carbon 39 (2001) 2247–2268.
[7] D.J. Ball, R.G. Stack, SAE 902 (1990) 110, Technical Paper.
[8] B.A.A.L. Van Setten, M. Makkee, J.A. Moulijn, Catal. Rev. Sci. Eng. 43 (2001) 489.
[9] K. Hinot, H. Burtscher, A.P. Weber, G. Kasper, Appl. Catal. B 71 (2007) 271.
[10] K.N. Pattas, C.C. Michalopoulou, SAE Paper 920362, 1992.
[11] G. Lepperhoff, H. Luders, P. Barthe, J. Lemaire, SAE Paper 950369, 1995.
[12] H. An, C. Kilroy, P.J. McGinn, Catal. Today 98 (2004) 423.
[13] C.A. Querini, L.M. Cornaglia, M.A. Ulla, E.E. Miro, Appl. Catal. B 20 (1999) 165.
[14] M.L. Pisarello, V. Milt, M.A. Peralta, C.A. Querini, E.E. Miro, Catal. Today 75 (2002) 465.
[15] R. Jimenez, X. Garcia, C. Cellier, P. Ruiz, A.L. Gordon, Appl. Catal. A 314 (2006) 81.
[16] D. Fino, N. Russo, G. Saracco, V. Specchia, J. Catal. 217 (2003) 367.
[17] B.A.A.L. van Setten, C.G.M. Spitters, J. Bremmer, A.M.M. Mulders, M. Makkee, J.A. Moulijn, Appl. Catal. B 42 (2003) 337.
[18] B.J. Cooper, J.E. Thoss, SAE Paper 890404, 1989.
[19] K. Yamazaki, T. Kayama, F. Dong, H. Shinjoh, J. Catal. 282 (2011) 289–298.
[20] S. Changsheng, P.J. McGinn, Appl. Catal. B 138 (2013) 70–78.
[21] P. Doggali, F. Grasset, O. Cador, S. Rayalu, Y. Teraoka, N. Labhsetwar, J. Environ. Chem. Eng. 2 (2014) 340–343.
[22] Z. Zhang, Y. Zhang, Z. Wang, X. Gao, J. Catal. 271 (2010) 12–21.
[23] S. Bensaid, N. Russo, D. Fino, Appl. Catal. B 152 (2014) 99–107.
[24] G. Marban, I. Lopez, T. Valdes-Solis, Appl. Catal. A 361 (2009) 160–169.
[25] L. Liu, Y. Chen, L. Dong, J. Zhu, H. Wan, B. Liu, B. Zhao, H. Zhu, K. Sun, L. Dong, Y. Chen, Appl. Catal. B 90 (2009) 105–114.
[26] K. Krishna, A. Bueno-Lopez, M. Makkee, J.A. Moulijn, Appl. Catal. B 75 (2007) 210–220.
[27] A. Avgouropoulosa, T. Ioannidesa, H. Matralis, Appl. Catal. B 56 (2005) 87–93.
[28] A. Martinez-Arias, A.B. Hungria, G. Munuera, Appl. Catal. B 65 (2006) 207–216.
[29] L. Liu, Z. Yao, B. Liu, J. Catal. 275 (2010) 45–60.
[30] G. Aguila, F. Garcia, P. Araya, Appl. Catal. A 343 (2008) 16–24.
[31] L.F. Liotta, A. Macaluso, A. Longo, G. Pantaleo, A. Martorana, G. Deganello, Appl. Catal. A 240 (2003) 295–307.
[32] S. Damyanova, B. Pawelwc, K. Arishtirova, M.V.M. Huerta, J.L.G. Fierro, Appl. Catal. A 337 (2008) 86–96.
[33] A. Martinez-Arias, R. Cataluna, J.C. Conesa, J. Soria, J. Phys. Chem. B 102 (1998) 809–817.
[34] H. Yahiro, M. Iwamoto, Appl. Catal. A 163 (2001) 163–181.
[35] G. Mul, J.P.A. Neeft, F. Karteijn, J.A. Moulijn, Carbon 36 (1998) 1269–1276.
[36] M.J.L. Gines, N. Amadeo, M. Laborde, C.R. Apesteguia, Appl. Catal. A 131 (1995) 283–296.
[37] T. Shishido, M. Yamamoto, D. Li, Y. Tian, H. Morioka, M. Honda, T. Sano, K. Takehira, Appl. Catal. A 303 (2006) 62–71.
[38] W.X. Pan, R. Cao, D.L. Roberts, G.L. Griffin, J. Catal. 114 (1988) 440–446.
[39] K.C. Waugh, Catal. Today 15 (1992) 51–75.
[40] J.S. Lee, K.H. Lee, S.Y. Lee, Y.G. Kim, J. Catal. 144 (1993) 414–424.
[41] S. Fujita, M. Usui, H. Ito, N. Takezawa, J. Catal. 157 (1995) 403–413.
[42] J. Nakamura, Y. Choi, T. Fujitani, Top. Catal. 22 (2003) 277–285.
[43] J.G. Nunan, C.E. Bogdan, K. Klier, C.W. Young, R.G. Herman, J. Catal. 116 (1989) 195–221.
[44] I. Boz, M. Sahibzada, I.S. Metcalfe, Ind. Eng. Chem. Res. 33 (1994) 2021–2028.
[45] A.M. Hilmen, M. Xu, M.J.L. Gines, E. Iglesia, Appl. Catal. A 169 (1998) 355–372.
[46] S.S. Fu, G.A. Somorjai, J. Phys. Chem. 96 (1992) 4542–4549.
[47] W.H. Cheng, Appl. Catal. A 130 (1995) 13–30.
[48] J.Y. Xi, Z.F. Wang, G.X. Lu, Appl. Catal. A 225 (2002) 77–86.
[49] A.Y. Rozovskiil, G.I. Lin, Top. Catal. 33 (2003) 137–150.
[50] M.V. Twigg, M.S. Spenser, Top. Catal. 22 (2003) 191–203.
[51] J. Agrell, K. Hasselbo, K. Jansson, S.G. Jaras, M. Boutonnet, Appl. Catal. A 211 (2001) 239–250.
[52] R.M. Navarro, M.A. Peña, J.L.G. Fierro, J. Catal. 212 (2002) 112–118.
[53] L.A. Espinoza, R.M. Lago, J.L.G. Fierro, Top. Catal. 22 (2003) 245–251.
[54] M.M. Gunter, T. Ressler, R.E. Jentoft, B. Bems, J. Catal. 203 (2001) 133–149.
[55] Y. Choi, H.G. Stenger, Appl. Catal. B 38 (2002) 259–269.
[56] H. Purnama, T. Ressler, R.E. Jentoft, H. Soerijanto, R. Schlogl, R. Schomacker, Appl. Catal. A 259 (2004) 83–94.
[57] G. Guan, T. Kida, T. Harada, M. Isayama, A. Yoshida, Appl. Catal. A 249 (2003) 11–18.
[58] J.P. Breen, H. Ross, Catal. Today 51 (1999) 521–533.
[59] B.A. Peppley, J.C. Amphlett, L.M. Kearns, R.F. Mann, Appl. Catal. A 179 (1999) 21–29.
[60] G. Fierro, M. Lo-Jacono, M. Inversi, P. Porta, F. Cioci, R. Lavecchia, Appl. Catal. A 137 (1996) 327–348.
[61] T.L. Reitz, P.L. Lee, K.F. Czaplewski, J.C. Lang, K.E. Popp, H.H. Kung, J. Catal. 199 (2001) 193–201.
[62] H. Oguchi, H. Kanai, K. Utani, Y. Matsumuira, S. Imamura, Appl. Catal. A 293 (2005) 64–70.

[63] T. Fujitani, J. Nakamura, Appl. Catal. A 191 (2000) 111–119.
[64] T. Shishido, M. Yamamoto, D. Li, Y. Tian, H. Morioka, M. Honda, K. Takiki, K. Takehira, Appl. Catal. A 303 (2006) 62–71.
[65] T. Shishido, M. Yamamoto, I. Atake, D. Li, Y. Tian, H. Moroika, M. Honda, T. Sano, K.J. Takehira, Appl. Catal. A 253 (2006) 270–278.
[66] G. Corro, U. Pal, E. Ayala, E. Vidal, E. Guilleminot, Top. Catal. 56 (2013) 467–472.
[67] M. Salamanca, F. Mondragon, J.R. Agudelo, P. Benjumea, P.A. Santamaria, Combust. Flame 159 (2012) 1100–1108.
[68] L.J. Bellamy, The Infrared Spectra of Complex Molecules, Chapman and Hall, London, 1975.
[69] G. Cordoba, R. Arroyo, J.L.G. Fierro, M. Viniegra, J. Solid State Chem. 123 (1996) 93–101.
[70] F. Boccuzzi, S. Coluccia, G. Martra, N. Ravasio, J. Catal. 184 (1999) 316–324.
[71] S. Velu, K. Susuki, M. Okazaki, M.P. Kapoor, T. Osaki, F. Ohashi, J. Catal. 194 (2000) 373–380.
[72] L.E. Orgel, J. Chem. Soc. 48 (1958) 4186–4199.
[73] K.M. Mertz, R. Hoffman, Inorg. Chem. 27 (1988) 2120–2128.
[74] Z.Y. Tan, D.W.Y. Yong, Z. Zhang, H.Y. Low, L. Chen, W.S. Chin, J. Phys. Chem. C 117 (2013) 10780–10787.
[75] S. Morpurgo, M.L. Jacono, P. Porta, J. Mater. Chem. 4 (1994) 197–205.
[76] S.C. Singh, R. Gopal, Bull. Mater. Sci. 30 (2007) 291–293.
[77] L. Martin, H. Martinez, D. Poinot, B. Pequenard, F. Le Cras, J. Phys. Chem. 117 (2013) 4421–4430.
[78] D. Briggs, M.P. Seah (Eds.), Practical Surface Analysis by Auger and X-ray Photoelectron Spectroscopy, 2nd ed., Wiley, Chichester, UK, 1990.
[79] E. Sasaoka, S. Hirano, S. Kasaoca, Y. Sakata, Energy Fuels 8 (1994) 763–769.
[80] J.A. Rodriguez, J.Y. Kim, J.C. Hanson, M. Perez, A.I. Frenkel, Catal. Lett. 85 (2003) 247–254.
[81] S. Galvagno, C. Crisafulli, R. Maggiore, G.R. Tauszik, A.T. Giannetto, Therm. Anal. 30 (1985) 611–618.
[82] Y. Okamoto, K. Fukina, T. Imanaka, S. Teranishi, J. Phys. Chem. 87 (1983) 3747–3754.
[83] K. Villani, R. Brosius, J.A. Martens, J. Catal. 236 (2005) 172–181.
[84] E. Aneggi, J. Llorca, C. Leitenburg, G. Dolcetti, A. Trovarelli, Appl. Catal. B 91 (2009) 489–497.
[85] F.E. López-Suárez, A. Bueno-López, M.J. Illán-Gómez, Appl. Catal. B 84 (2008) 651–658.
[86] R.G. Herman, K. Klier, G.W. Simmons, B.P. Finn, J.B. Bulko, J. Catal. 56 (1979) 407–429.